富山大学水素同位体機能研究センター研究報告17：61－71，1997

論　文

焼結型 Mg_2Ni の充放電特性

舒　衛民・水上憲三・渡辺国昭・諸住正太郎

富山大学水素同位体機能研究センター
〒930-8555 富山市五福 3190

Charge/Discharge Characteristics of Sintered Mg_2Ni

W. M. SHU, K. MIZUKAMI, K. WATANABE and S. MOROZUMI

Hydrogen Isotope Research Center, Toyama University
Gofuku 3190, Toyama 930-8555, Japan

(Received November 19, 1997; accepted March 9, 1998)

Abstract

The charge/discharge characteristics of sintered Mg_2Ni as an anode of nickel/metal hydride battery were studied with an electrochemical cell. The discharge capacity of sintered Mg_2Ni increases initially with the charge/discharge cycles. Cycle life (CL) for sintered samples is much greater than that of the un-sintered sample, and the largest CL appears at the sintering temperature of 550°C. The effects of sintering temperature on CL degradation were examined through the changes in the specific surface area and the chemical composition. The sample sintered at 550°C holds the largest specific surface area, and the segregation of Mg over the outside layer of samples was confirmed for those sintered at temperatures higher than 550°C. The degradation after charge/discharge cycling was investigated with X-ray diffraction and scanning electron microscopy. The XRD pattern shows a new phase of $Mg(OH)_2$ besides the phase of Mg_2Ni after charge/discharge cycling. It indicates that the formation of $Mg(OH)_2$ at the outside layer of samples contributes to the degradation of the anode performance.

1. Introduction

Rare earth (AB_5) [1-4] and Laves-phase (AB_2) [5-7] hydrogen storage alloys electrochemically absorb and desorb reversibly a large amount of hydrogen in an alkaline solution. When the metal hydride anode is combined with a nickel cathode, a rechargeable battery is realized, where charge and discharge reactions are not accompanied by the dissolution and precipitation of active materials and then by the consumption and production of water [1-7]. The nickel-hydrogen batteries have some inherent advantages over conventional rechargeable batteries with respect to discharge capacity, cleanliness and tolerance to overcharge and overdischarge [1-3].

Magnesium and magnesium-based alloys are known to have much higher hydrogen absorbability than conventional hydrogen storage alloys such as AB_5 and AB_2, in addition to their lower specific gravity and richer natural resources [8-12]. In comparison with the conventional hydrogen storage alloys, however, magnesium and magnesium-based alloys need to be operated at much higher temperatures because of their lower equilibrium pressure and poorer surface activity [11, 12]. To improve the surface activity of Mg-based alloys, a surface treatment technique using a fluorine-containing aqueous solution, the so called F-treatment technique was developed [13]. It was found that the F-treatment could clean up surface layers of MgO and/or $Mg(OH)_2$ and form a porous, water insoluble MgF_2 top-layer overlapping a metallic Ni-riched substrate, resulting in an extremely high hydrogen affinity [13]. On the other hand, Orimo et al. [14, 15] reported that a nano-structured composite material of Mg_2Ni-H system synthesized by reactive grinding could absorb and desorb hydrogen at temperatures lower than 100°C.

It was recently found that some amorphous Mg-Ni alloys prepared by mechanical alloying can adsorb and desorb electrochemically a large amount of hydrogen at room temperature [16]. This makes it a very promising material for Ni-metal hydride rechargeable batteries. However, the degradation of its discharge capacity is much faster that that of AB_5, AB_2 and AB-type metal hydride electrodes. X-ray diffraction and X-ray photoelectron spectroscopy results indicated that serious oxidation of magnesium and nickel occurred on amorphous Mg_2Ni, which was regarded as the main reason for its capacity degradation [16, 17].

In this work, as a new anode preparation technique, Mg_2Ni powder was sintered at various sintering temperatures. The sintered Mg_2Ni without any binder was electrochemically

characterized in order to evaluate briefly its possibility as anode material in nickel-metal hydride batteries. In addition, the effects of sintering temperature upon the hydride anode performance were examined by the measurement of specific surface area and the analysis of chemical composition, and the degradation after charge/discharge cycling was investigated by X-ray diffraction and scanning electron microscopy.

2. Experimental

In the Mg-Ni system, there are two intermetallic compounds, Mg_2Ni and $MgNi_2$. The latter does not react with hydrogen, at least up to temperatures of 350°C and pressures of 2.8 MPa, whereas the former reacts readily with hydrogen at 325°C and 2.1 MPa, producing a ternary hydride with the formula of Mg_2NiH_4 [11, 12]. The material used in this study was Mg_2Ni powder (below 200 mesh) purchased from Japan Metal & Chemicals Corporation. Two types of samples were prepared in order to investigate the effects of sample preparation. Sample 1 (0.2 g) was first pressed into a disk of 10 mm in diameter and 1 mm in thickness by a force of 40 MPa, then sintered in an argon atmosphere at varying temperatures of 450 to 625°C, and finally sandwiched between nickel meshes as a current collector. Sample 2 (0.5 g), on the other hand, was first sandwiched between nickel meshes, then pressed into a rectangle of 15×20 mm, and finally sintered in an argon atmosphere at varying temperatures of 450 to 625°C.

Electrochemical measurements were conducted at room temperature by use of a nickel-hydrogen battery test system comprised of a battery charge/discharge unit (Hokuto Denko Corporation, HJ-201B). The test cell was filled with 6M KOH electrolyte solution. The test cathode was $NiOOH/Ni(OH)_2$, and the anode was sample 1 or sample 2. The total capacity of the cathode was much larger than that of the anode. The discharge capacity of the anode was expressed in mAh per gram of the alloy. Sample 1 was charged at 20 mA for 10 min, then rested for 10 min, and discharged at 5 mA to 0 V. For sample 2, on the other hand, the charge was set at 40 mA for 30 min, rest for 10 min, and discharge at 10 mA.

The apparatus to determine specific surface area consists of a vacuum pumping system, a gas supply system, a sample tube, a handmade ohmic heater and a measuring system. The residual pressure of the vacuum system was usually below 10^{-6} Pa. The reaction volume was calibrated by gas expansion. Prior to measurements, the sample was activated at 150°C for 2 hours by a temperature programmer connected to the heater. The surface areas were measured at liquid nitrogen temperature with krypton following the BET method.

The chemical compositions were measured by an energy dispersion spectrometer (EDS, EDAX 9100) and a X-ray spectrometer (XRS, Philips PW2300). The Mg content of the outside of the samples was measured by EDS. After EDS measurement, the samples were pulverized mechanically into powder, and then the Mg content of the inside of the samples (powder) was measured by XRS.

The crystallographic features of samples before and after charge/discharge cycles were measured by X-ray diffraction (XRD, Philips PW1700). Powder morphology was observed by scanning electron microscopy (SEM, EDAX 9100) before and after charge/discharge cycling.

3. Results and discussion

3.1. Cycle life

Mg_2Ni electrochemically absorbs and desorbs hydrogen in alkaline solution as a reversible anode. The overall reaction is written as

$$Mg_2Ni+4Ni(OH)_2 \rightleftharpoons Mg_2NiH_4+4NiOOH$$

Figure 1 shows a typical discharge curve, which was measured for sample 1 sintered at 475°C. It can be seen in the figure that the discharge capacity increases initially with the cycle number. This may be caused by the activation of alloy surfaces during the initial charge/discharge cycling. The maximum capacity appears at the cycle number of 16 for this sample.

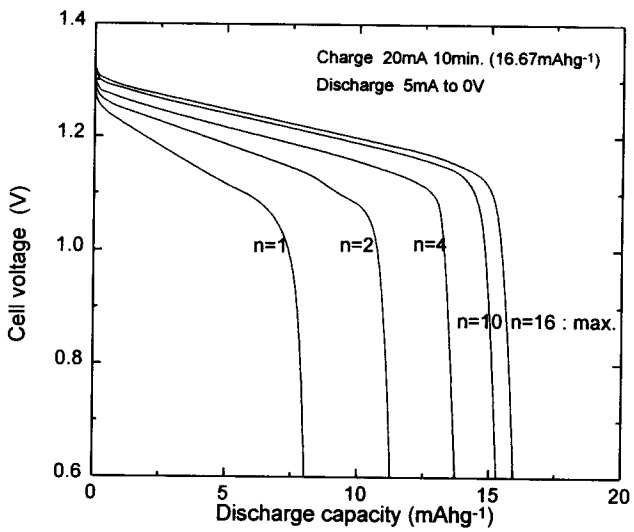

Fig. 1. The discharge curves of sample 1 sintered at 475°C for cycle numbers of 1, 2, 4 ,10 and 16.

Both samples 1 and 2 were sintered in argon atmosphere at varying temperatures. Figure 2 shows discharge characteristics of sample 1 for various sintering temperatures. The axis of coordinate is AHE (Ampere Hour Effect), *i.e.* the fraction of discharged capacity to charged capacity. A cycle life (CL) was defined here as cycle numbers at which the discharged capacity

decreased to a half of charged capacity. As shown in Fig. 2, CL for sintered samples was much greater than that of the un-sintered sample, and the largest CL (about 350) appeared at the sintering temperature of 550°C. In other words, CL increased initially with the increase in sintering temperature below 550°C, and then decreased with sintering temperature above 550°C.

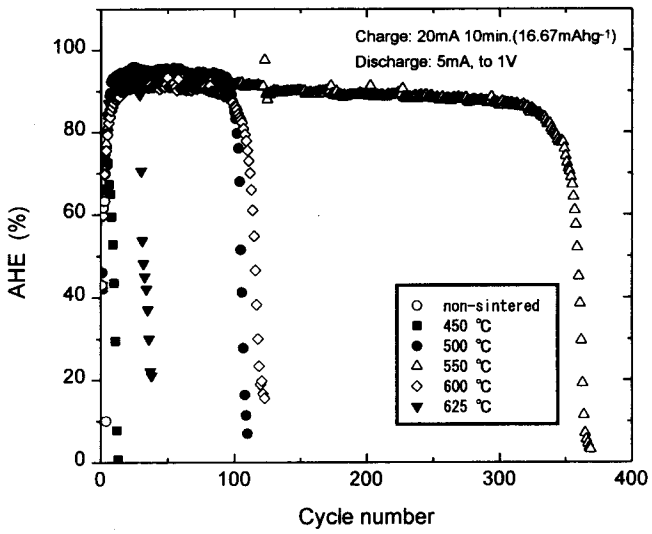

Fig. 2. The discharge characteristics of sample 1 for non-sintered and sintered at various temperatures.

For sample 2, the discharge characteristics are shown in Fig. 3 for the sintering temperatures of 500, 550, 600 and 650°C. Similarly, the largest CL appeared at the sintering temperature of 550°C. Figures 2 and 3 show that CL of sample 2 was smaller than that of sample 1 at the same sintering temperatures. However, the CL for sample 2 would be much larger than that of sample 1 if the charge and discharge condition were same for the two types of samples, considering that the charged capacity of sample 2 was a few times greater than that of sample 1, and that discharged current for sample 2 was double of that for sample 1.

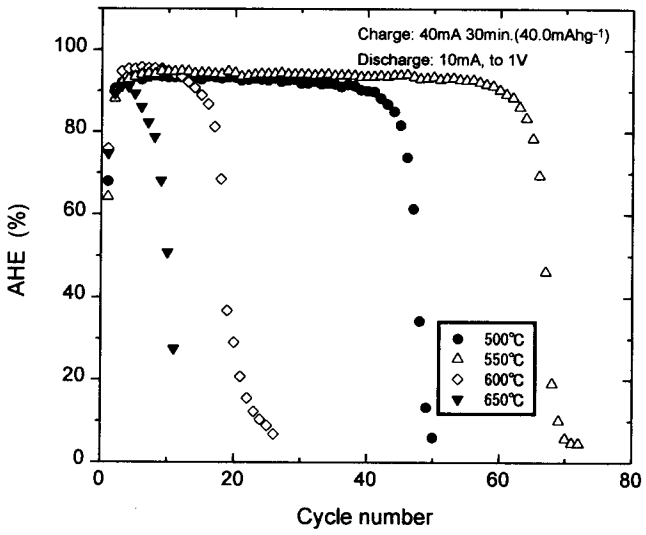

Fig. 3. The discharge characteristics of sample 2 sintered at 500, 550, 600 and 650°C.

The CL for the two types of samples is plotted against sintering temperature in Fig. 4. For

both samples 1 and 2, the largest CL appeared at the sintering temperature of 550°C. At temperatures lower than 550°C, the binding between the fine powders was so weak that some powder peeled off after a few cycles of charge and discharge. The reasons for the degradation at higher temperatures will be discussed in the next subsection.

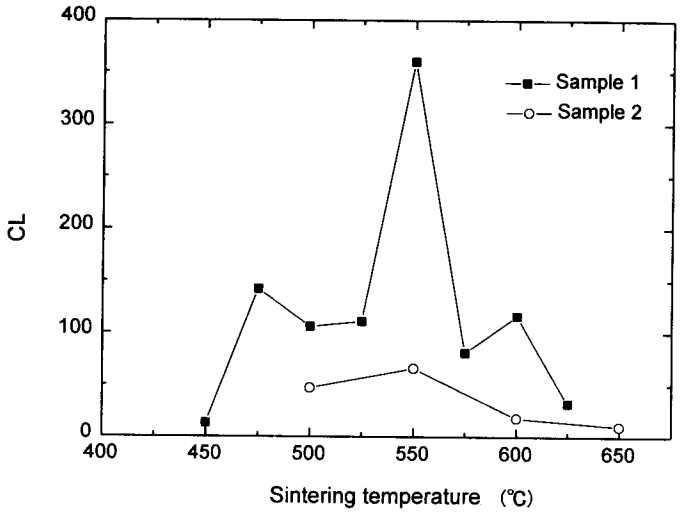

Fig. 4. The dependence of the cycle life on sintering temperature for two types of samples.

3.2. Degradation at higher temperature

As shown in Fig. 4, the CL for the two types of samples sintered at temperatures higher than 550°C was smaller than that of 550°C. The degradation of anode performance for samples sintered at higher temperatures was examined through the measurement of specific surface area and the analysis of chemical compositions.

The specific surface areas determined by BET method are shown in Fig. 5 for the un-sintered sample (dashed line) and those sintered at 500, 550 and 600°C, with an error of 0.5%. The specific surface area sintered at 500°C was a little larger than that of the un-sintered sample, and a maximum appears at 550°C. For the sample sintered at 600°C, however, the specific surface area was even smaller

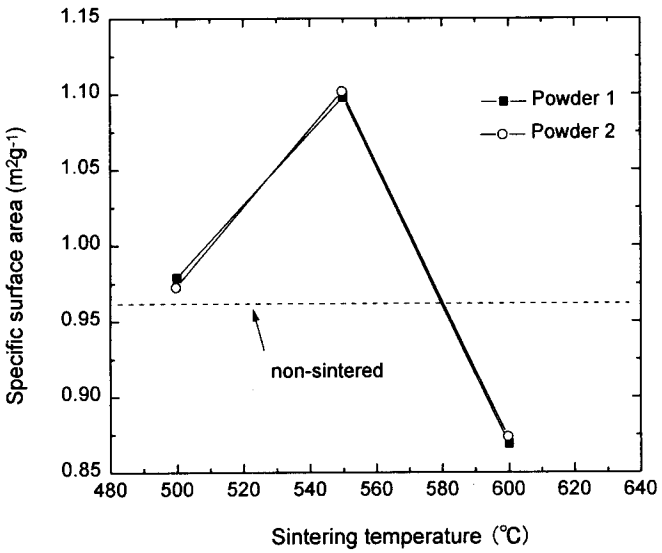

Fig. 5. The specific surface areas for samples un-sintered and sintered at 500, 550 and 600°C.

than that of the un-sintered sample. The decrease in specific surface area was one of the reasons of the CL degradation for the samples sintered at temperatures higher than 550°C.

The chemical compositions were measured by both EDS (the outside of the samples) and XRS (the inside of the samples). The relative changes in Mg content of sintered samples to the un-sintered sample are plotted in Fig. 6 against sintering temperature. The X-ray spectrometer results show that the inside Mg-content drops about 7 to 12 wt% for sintered samples comparing with the un-sintered one. The EDS results, however, show that the outside Mg-content was larger for sintered sample than that of the un-sintered, except the sample sintered at 500°C. Specially, the sample sintered at 650°C shows Mg enrichment by about 10 wt% at the outside layer. The Mg segregation at the outside layer contributes to the CL degradation of the samples sintered at temperatures higher than 550°C.

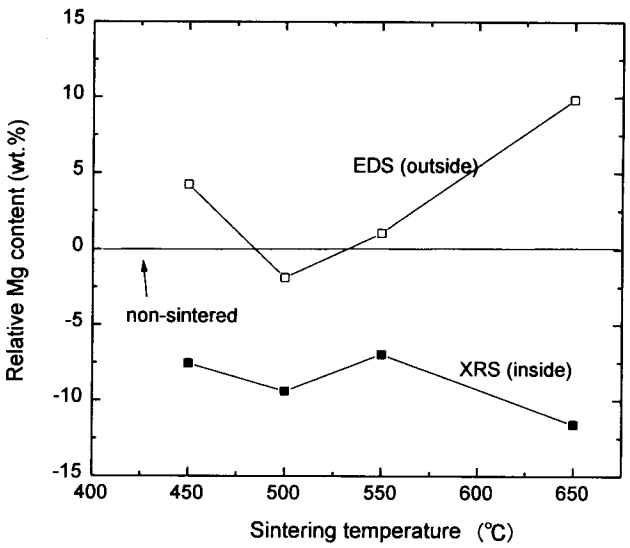

Fig. 6. The relative changes in Mg content of sintered samples comparing with the un-sintered sample.

3.3. Degradation with cycling

The degradation with charge/discharge cycling was investigated by XRD and SEM for the samples before and after cycling. Fig. 7 shows the XRD results of sample 2 sintered at 550°C. The as-prepared sample was pulverized mechanically into powder after sintering and then the powder was measured by XRD. Similarly, the sample after cycling was pulverized mechanically into powder after 70 cycles for XRD measurement. The XRD results indicates that a single phase of Mg_2Ni exists in the as-prepared sample while there appears a new phase of $Mg(OH)_2$ besides the phase of Mg_2Ni in the sample of after charge/discharge cycling.

It is well-known that the hydrogen absorbing and desorbing cycles bring about the pulverization of the alloy, continuously enlarged surface area, and production of fresh surface and the formation of oxide or hydroxide. Therefore, the repeated charging and discharging in

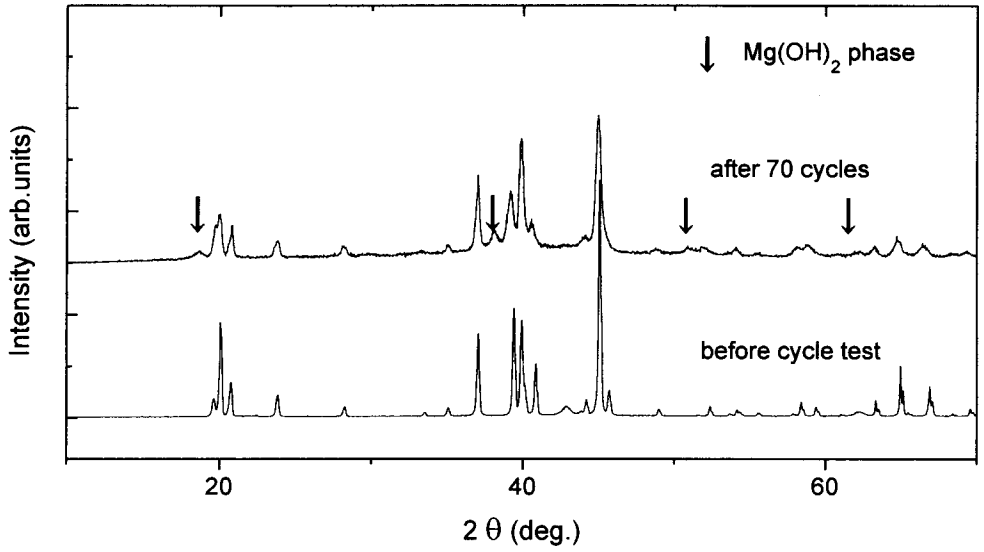

Fig. 7. The X-ray powder diagrams before and after charge/discharge cycling for sample 2 sintered at 550°C.

KOH solution caused continuous degradation of the alloy. Hydrogen storage capacity of a $LaNi_5$ anode was reduced to as much as 40% of the initial value after only 100 charge/discharge cycles due to the decomposition of $LaNi_5$ to $La(OH)_3$ and Ni [2]. Willems et al.[1] have found that the anodes of $LaNi_{2.5}Co_{2.5}$-based alloys have much longer cycle life than $LaNi_5$ or its ternary alloys, though the replacement of Ni by Co brought about a considerable decrease in hydrogen storage capacity. They argued that the significant improvement of durability was closely associated with the reduction of volume expansion ratio of the alloy to its hydride [1]. Sakai et al. [18, 19] have reported that the surface coating of pulverized $LaNi_5$ by porous copper or nickel was very useful for increasing the cycle life, because the coated metal film works as both an

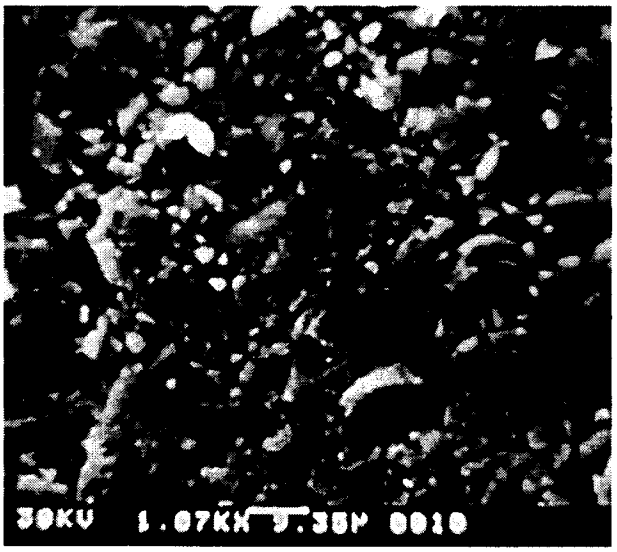

Fig. 8. SEM morphology before charge/discharge cycling.

oxidation barrier to protect the metal hydride and a micro current collector for proceeding electrochemical reactions on the surface.

It is thus deduced that the presence of $Mg(OH)_2$ in the sintered Mg_2Ni degrades the anode performance. Therefore, the prevention of the formation of oxide or hydroxide in the sintered Mg_2Ni samples is one of the most important tasks.

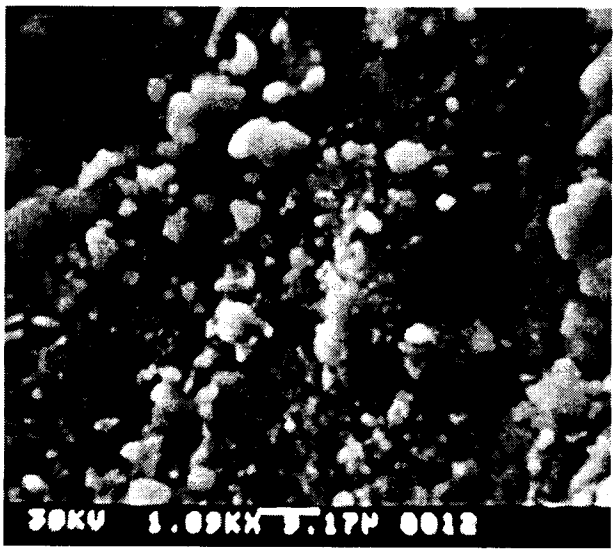

Fig. 9. SEM morphology after charge/discharge cycling.

SEM morphology of sample 2 before and after charge/discharge cycling is shown in Figs. 8 and 9. The powder particles on the outside of the sample before charge/discharge cycling have definite boundaries, while those after cycle test became a little vague. This difference may be attributed to the formation of $Mg(OH)_2$ during the charge/discharge cycling.

4. Conclusions

The charge/discharge cycling experiments show that the sintered Mg_2Ni is a promising anode material. The results of the present study are summarized as the following:

(1) The discharge capacity increased initially with the cycle number, indicating that the activation of the anode surface occurs during the initial charge/discharge cycling.

(2) A cycle life (CL) for sintered samples was much larger than that of the un-sintered sample, and the largest CL appeared at the sintering temperature of 550°C. At temperatures lower than 550°C, the weak binding between the fine powders is the main reason for small CL. The decrease in specific surface area and Mg segregation at the outside layer contribute to the CL degradation for the samples sintered at temperatures higher than 550°C.

(3) A new phase of $Mg(OH)_2$ appeared after charge/discharge cycling besides the original phase of Mg_2Ni. It suggests that the phase of $Mg(OH)_2$ at the outside layer of samples degrades the anode performance.

Acknowledgment

The authors are indebted to Dr. K. Matsuda (Faculty of Engineering, Toyama University) for operating SEM/EDS instruments. They are also grateful for a gift of the cathode material to Human Environmental Systems Development Center of Nationanl/Panasonic Co. and for that of the anode alloy to Japan Metals and Chemicals Co.

References

1) J. J. G. Willems and K. H. J. Buschow, J. Less-Common Met., **129** (1987) 13.
2) T. Sakai, H. Miyamura, N. Kuriyama, A. Kato, K. Oguro and H. Ishikawa, J. Electrochem. Soc. **137 (3)** (1990) 795.
3) X. H. Wang, C. P. Chen, C. S. Wang and Q. D. Wang, J. Alloys & Compounds, **232** (1996) 192.
4) C. Iwakura, T. Oura, H. Inoue and M. Matsuoka, Electrochimica Acta, **41** (1996) 117.
5) S. R. Ovshihsky, M. A. Fetcenko and J. Ross, Science, **260** (1993) 176.
6) J. Huot, E. Akiba, T. Ogura and Y. Ishido, Denki Kagaku, **61** (1993) 1424.
7) H. Miyamura, T. Sakai, N. Kuriyama, K. Oguro, I. Uehara and H. Ishikawa, Z. Phys. Chem., **183** (1994) 347.
8) J. J. Reilly and R. H. Wiswall, Inorg. Chem. **7** (1968) 2254.
9) Z. Gavra, M. H. Mintz, G. Kimmel and Z. Hadari, Inorg. Chem. **18** (1979) 3595.
10) J. Genossar and P. S. Rudman, J. Phys. Chem. Solids, **42** (1981) 611.
11) D. Noreus, K. Jansson and M. Nygren, Z. Phys. Chem., **146** (1985) 191.
12) D. Noreus and L. Kihlborg, J. Less-Common Met., **123** (1986) 233.
13) F. J. Liu and S. Suda, J. Alloys & Compounds, **232** (1996) 212.
14) S. Orimo and H. Fujii, J. Alloys & Compounds, **232** (1996) L16.
15) S. Orimo, H. Fujii and K. Ikeda, Acta Mater., **45** (1997) 331.
16) Y. Q. Lei, Y. M. Wu, Q. M. Yang, J. Wu and Q. D. Wang, Z. Phys. Chem., **183** (1994) 379.
17) D. L. Sun, Y. Q. Lei, W. H. Liu, J. J. Jiang, J. Wu and Q. D. Wang, J. Alloys & Compounds, **231** (1995) 621.
18) T. Sakai, K. Ishikawa, K. Oguro, C. Iwakura and H. Yoneyama, J. Electrochem. Soc.

134 (1987) 558.

19) C. Iwakura, Y. Kajiya, H. Yoneyama, T. Sakai, K. Oguro and H. Ishikawa, J. Electrochem. Soc. **136** (1989) 1351.